Numerical framework for pattern-forming models on evolving-in-time surfaces

Andriy Sokolov[a], Robert Strehl[b], Ramzan Ali[a], Stefan Turek[a]

[a] *Institut für Angewandte Mathematik, TU Dortmund, Vogelpothsweg 87, 44227 Dortmund, Germany*
[b] *Department of Mathematics, Ryerson University, Toronto, ON, M5B 2K3, Canada*

Abstract

In this article we apply an earlier developed numerical framework to Turing-type reaction-diffusion equations on an evolving-in-time hypersurface Γ. The proposed framework combines the level set methodology for the implicit description of the time dependent Γ, the Eulerian finite element formulation for the numerical treatment of partial differential equations and an optional flux-corrected transport scheme for the numerical stabilization of arising advective, resp., convective terms. Major advantages of this scheme are that it avoids numerical calculation of curvature, allows interaction of surface-defined partial differential equations with domain-defined partial differential equations through the level set bulk and preserves the positivity of the solution through the algebraic flux correction. The corresponding numerical tests demonstrate the ability of the scheme to deliver an acceptably accurate solution with a reasonably good convergence behavior.

Keywords: chemotaxis; Turing instability; pattern formation; level set; FEM.

1. Introduction

In numerous biological and medical applications there is a necessity of understanding and predicting the dynamics of cells and species during pattern-forming

Email addresses: asokolow@math.tu-dortmund.de (Andriy Sokolov), rstrehl@ryerson.ca (Robert Strehl), ramzan.ali@math.tu-dortmund.de (Ramzan Ali), ture@featflow.de (Stefan Turek)

processes. Among them are, for example, the coloring of animal coats [22, 21, 23, 41, 5, 16] or dynamics of the yeast cell polarity [15, 29]. Mathematically, this kind of processes can be described by systems of reaction-diffusion equations of a Turing-instability type which, firstly observed and studied by A. Turing in 1952 in his pioneering paper [37], provides a prominent mechanism for pattern formation in biological, physical, ecological and chemical systems.

A large class of biological application requires extension of reaction-diffusion systems by some advective and/or convective terms. Here, the spatial dynamics of cells and species are greatly influenced by transport-driven mechanisms. An example of such mechanisms are models for chemotaxis. Firstly described by E. Keller and L. Segel in 1971 [17, 18], chemotaxis models are currently widely used to describe bacteria/cells aggregation and formation processes [1, 20, 38, 39, 40], modeling of tumor invasion and metastasis processes before a proliferation dominated stage [4, 9, 3, 8, 7], modeling of vasculogenesis [2, 14, 30], etc. In multicellular organisms chemotaxis is vitally important across all stages of their life cycle. Chemotaxis has particular applications in gastrulation, patterning of nervous system (e.g., Park et al. [27]) and migration of immune cells in healing and inflammation, e.g., [42]. The same mechanisms are used during cancer growth to invade the surrounding healthy environment by tumor cells, see, e.g., [10, 4, 9, 3, 8, 7], etc.

Very often we have to treat reaction-diffusion-advection processes on some surface: this can be a skin of an animal, a shape of an amoeba or a bacteria, a membrane of a cell, etc. From a macroscopic point of view this leads to the biological-medical applications whose mathematical description contains partial differential equations (PDEs) on surfaces. Currently, PDEs on surfaces vastly increase in popularity and therefore is a rapidly developing topic. It has a wide range of application in engineering [32], image processing [35], computer graphics [13, 43], etc. Among the variety of biological applications which deal with surfaces-defined PDEs prominent examples are chemotaxis-related processes on stationary and deforming manifolds [19, 12], protein dynamics on a cell membrane [15, 29] and coloring patterns on growing surfaces [5, 16, 6].

One general mathematical model which could mainly encompass all examples mentioned above can be formulated by the following system of reaction-advection-diffusion equations:

$$\frac{\partial c_i}{\partial t} = D_i^c \Delta c_i - \nabla \cdot [\chi_i^c \boldsymbol{w}_i^c(\boldsymbol{c}, \boldsymbol{\rho}) c_i] + f_i(\boldsymbol{c}, \boldsymbol{\rho}), \text{ in } \Omega \times T\,, \tag{1}$$

$$\frac{\partial^* \rho_j}{\partial t} = D_j^\rho \Delta_{\Gamma(t)} \rho_j - \nabla_{\Gamma(t)} \cdot (\chi_j^\rho \boldsymbol{w}_j^\rho(\boldsymbol{c}, \boldsymbol{\rho}) \rho_j) + g_j(\boldsymbol{c}, \boldsymbol{\rho}), \text{ on } \Gamma(t) \times T\,, \tag{2}$$

where $\partial^* \rho_j / \partial t$ is a time derivative which takes into account the evolution of $\Gamma(t)$ and will be detailed in the next section. The corresponding boundary and initial conditions are yet to be provided. Here, $c_i(\boldsymbol{x}, t)$, $i = 1 \dots n$, are defined in the whole space-time domain $\Omega \times T$ and are solutions of (1). The unknown functions $\rho_j(\boldsymbol{x}, t)$, $j = 1 \dots m$, are however defined on the surface-time domain $\Gamma(t) \times T$ and are solutions of (2). Here and for the remainder we assume that the evolution of the surface does not exceed the underlying stationary domain, i.e., $\Gamma(t) \subset \Omega$. We adopt the notation to write multi dimensional vectors in bold letters, e.g., $\boldsymbol{c} = (c_1, \dots, c_n)^T$. The position of $\Gamma(t)$ is implicitly provided by the zero level set (LS) of the time dependent level set function $\phi(\boldsymbol{x}, t)$ those values are either given analytically or found by solving the transport equation

$$\frac{\partial \phi}{\partial t} + \boldsymbol{v} \cdot \nabla \phi = 0\,, \tag{3}$$

where $\boldsymbol{v}$ is the velocity of the surface. By the proper choice of numbers of equations n and m, parameters D_i^c and D_j^ρ, chemotaxis/advection-related functions $\boldsymbol{\chi}_i^c$ and $\boldsymbol{v}_i^c$, as well as kinetic terms $f_i(\cdot)$ and $g_j(\cdot)$, we can mainly reobtain one of the models presented in the above references.

The current article treats the construction of a numerical scheme for the system of PDEs (2)–(3). Namely, we focus on a numerical scheme for pattern-forming systems of Turing-instability type, which consist of two coupled reaction-diffusion equations on evolving-in-time surface $\Gamma(t)$:

$$\frac{\partial^* \rho_1}{\partial t} = D_1^\rho \Delta_{\Gamma(t)} \rho_1 + g_1(\rho_1, \rho_2), \text{ on } \Gamma(t) \times T\,, \tag{4}$$

$$\frac{\partial^* \rho_2}{\partial t} = D_2^\rho \Delta_{\Gamma(t)} \rho_2 + g_2(\rho_1, \rho_2), \text{ on } \Gamma(t) \times T\,, \tag{5}$$

where the position of $\Gamma(t)$ is prescribed implicitly by the level set function ϕ, which is a subject to (3). Note that we focus only on equations on an evolving-in-time surface of kind (2). However the reader will recognize that a coupling with equations in the whole space-time domain $\Omega \times T$, e.g., equations of kind (1), is readily promoted by our computational framework.

The development of an efficient computational framework for (1)–(3) is a demanding task. Let us point to the major challenges and outline how we aim to tackle them.

Discretization of the evolving-in-time surface A robust discretization approach for a PDE on a non-stationary surface $\Gamma(t)$ needs special handling. Particularly when a adaptive spatial discretization is mandatory. In a previous article [31] the authors proposed a finite element level set based methodology (FE-LS scheme). Therein it is documented that this approach provides sufficiently accurate solutions for exemplary test cases. A main benefit of this approach is the shared discretization ansatz for the domain-defined and surface-defined PDEs via the ε-band around the zero level set. This simplifies the coupling between the two different PDE domains of definition. Moreover (as sketched in a next section) the costly calculation of the mean curvature is obsolete in this approach.

Numerical stabilization As known from transport-dominant equations numerical

schemes may suffer from artificially introduced oscillatory solution profiles and non positivity preservation. In our case such numerical pollutions might be introduced by chemotaxis processes, transport of species/quantities and the evolution of the surface. In order to counter the occurrences of this effect we use the linearized FCT/TVD stabilization that has already been successfully applied in [34, 33, 31].

Sensitivity of the Turing system Because of the system sensitivity in terms of the emergence of certain patterns, the numerical treatment of the cou-

pling of the underlying systems' equations is of particular importance. A suitable iteration strategy should account for a justified treatment of the nonlinearities in the system that strongly influence the dynamical behavior of the solution.

The main contribution of the current article is to present new applications of the previously developed framework [31] to models that exhibit Turing-type instabilities. This contribution also presents a accurate linearization strategy for the nonlinear reaction terms arising in those models which is crucial to capture the parameter sensitivity (as already mentioned above).
The article is organized as follows. In Section 2 we will briefly describe the implicit finite element level set based scheme. Then, in Section 2.4 we construct a numerical scheme for the systems of reaction-diffusion equations of the Turing-instability type on evolving-in-time surfaces. After that in Section 3 we show numerical results for Turing systems on deforming surfaces and discuss properties of the proposed numerical scheme. Section 4 summarizes the characteristics of the approach, draw the concluding remarks and discuss the future work to be done in this direction.

2. Implicit FE-LS scheme

The formulation of our scheme follows the lines in [31]. Particularly we let $\Gamma(t)$ be embedded in a stationary computational domain Ω that serves as 'bounding box' and is chosen large enough to cover $\Gamma(t)$ for all simulation time. This domain Ω will be the basis to discretize $\Gamma(t)$ in time. Note that in some cases it is sufficient only to consider a ε-band around the zero level set, i.e., we use Ω_ε as underlying domain to realize a discretization of equations of kind (2)–(3).

2.1. PDE on evolving hypersurface

The reaction-diffusion-convection/advection equation on an evolving-in-time surface $\Gamma(t)$ mathematically reads:

$$\frac{\partial^* \rho}{\partial t} = D\Delta_{\Gamma(t)}\rho - \nabla_{\Gamma(t)} \cdot (\boldsymbol{w}\rho) + g(\rho) \text{ on } \Gamma(t) \times T\,. \tag{6}$$

Here, the derivative

$$\frac{\partial^* \rho}{\partial t} = \partial_t^\bullet \rho + \rho \nabla_{\Gamma(t)} \cdot \boldsymbol{v}$$

is due to the evolution of $\Gamma(t)$ and can be obtained by the Leibniz formula

$$\frac{d}{dt}\int_{\Gamma(t)} \rho = \int_{\Gamma(t)} \partial_t^\bullet \rho + \rho \nabla_{\Gamma(t)} \cdot \boldsymbol{v}\,,$$

where $\partial_t^\bullet \rho = \partial_t \rho + \boldsymbol{v} \cdot \nabla \rho$ is the advective surface material derivative. The surface velocity $\boldsymbol{v} = V\boldsymbol{n} + \boldsymbol{v}_S$ can be decomposed into its velocity in the normal direction $V\boldsymbol{n}$, with $\boldsymbol{n}$ being a surface outward normal vector, and in the tangential direction $\boldsymbol{v}_S$. We can easily find that

$$V(\boldsymbol{x}, t) = -\frac{\phi_t(\boldsymbol{x}, t)}{|\nabla \phi(\boldsymbol{x}, t)|}\,.$$

Using the relations

$$\nabla_\Gamma \cdot \boldsymbol{v} = -VH + \nabla_\Gamma \cdot \boldsymbol{v}_S \quad \text{and} \quad \boldsymbol{v} \cdot \nabla \rho = V\frac{\partial \rho}{\partial \boldsymbol{n}} + \boldsymbol{v}_S \cdot \nabla \rho\,,$$

where H denotes the mean curvature, we can rewrite (6) as

$$\partial_t \rho + \boldsymbol{v}_S \cdot \nabla \rho - VH\rho + V\frac{\partial \rho}{\partial \boldsymbol{n}} + \rho \nabla_{\Gamma(t)} \cdot \boldsymbol{v}_S = D\Delta_{\Gamma(t)}\rho + g(\rho)$$

or, in terms of the surface material derivative, as

$$\partial_t^\bullet \rho + \rho \nabla_\Gamma \cdot \boldsymbol{v} = D\Delta_{\Gamma(t)}\rho - \nabla_{\Gamma(t)} \cdot (\boldsymbol{w}\rho) + g(\rho)\,.$$

2.2. Level set method

We assume that $\Gamma(t) \subset \Omega \subset \mathbb{R}^{d+1}$ is a compact connected and oriented d-dimensional hypersurface without boundary and that Γ is $\mathcal{C}^2$. Then, there exists

a two times continuously differential level set function $\phi : T \times \Omega \to \mathbb{R}$ defined by

$$\phi(t, \boldsymbol{x}) = \begin{cases} < 0 & \text{, if } \boldsymbol{x} \text{ is inside } \Gamma(t), \\ = 0 & \text{, if } \boldsymbol{x} \in \Gamma(t), \\ > 0 & \text{, if } \boldsymbol{x} \text{ is outside } \Gamma(t), \end{cases} \tag{7}$$

such that $|\nabla\phi| \neq 0$. An outward normal to $\Gamma(t)$ is

$$\boldsymbol{n} = (n_1, \ldots, n_{d+1})^T = \frac{\nabla\phi}{|\nabla\phi|} \tag{8}$$

and the matrix

$$\mathcal{P}_\Gamma = \left\{ \delta_{ij} - \sum_{j=1}^{d+1} n_i n_j \right\}_{ij} = I - \frac{\nabla\phi}{|\nabla\phi|} \otimes \frac{\nabla\phi}{|\nabla\phi|} \tag{9}$$

denotes the orthogonal projection onto the tangent space $\mathcal{T}_{\boldsymbol{x}}\Gamma$. Observe that if $\phi(\cdot)$ is chosen as a signed distance function then $|\nabla\phi| = 1$. For a scalar function ξ on Ω and a tangential vector field $\boldsymbol{\xi}$ on Γ one obtains

$$\nabla_\Gamma \xi = \mathcal{P}_\Gamma \nabla\xi = \left\{ \frac{\partial \xi}{\partial x_i} - \sum_{j=1}^{d+1} n_i n_j \frac{\partial \xi}{\partial x_j} \right\}_i , \tag{10}$$

$$\nabla_\Gamma \cdot \boldsymbol{\xi} = \sum_{i=1}^{d+1} \left(\frac{\partial \xi_i}{\partial x_i} - \sum_{j=1}^{d+1} n_i n_j \frac{\partial \xi_i}{\partial x_j} \right). \tag{11}$$

We would like to mention that for the natural extension, i.e., when ξ is constant along $\nabla\phi$, one can omit Γ in spatial differentiation on the right-hand-sides of (10) and (11). The Laplace-Beltrami operator on $\Gamma(t)$ with respect to the level set function ϕ can be written as

$$\Delta_\Gamma \xi = \nabla_\Gamma \cdot \nabla_\Gamma \xi = \nabla_\Gamma \cdot \mathcal{P}_\Gamma \nabla\xi. \tag{12}$$

The Eulerian mean curvature is defined through the level set function as

$$H = -\nabla_\Gamma \cdot \boldsymbol{n} = -\nabla_\Gamma \cdot \frac{\nabla\phi}{|\nabla\phi|}.$$

In the level set formulation one performs calculation not only on Γ, but indeed in a bulk ε-extension of the geometry of Γ which is denoted by Ω_ε. Herein

ε refers to the *width* or *thickness* of that extension. For the sake of brevity and simplicity, we assume that all considered in this article values/fields can be naturally, i.e., as a constant in a $\nabla\phi$-direction, extended to any level set

$$\Gamma(t)_c = \{\boldsymbol{x} \in \Omega_\varepsilon : \phi(t, \boldsymbol{x}) = c\}, \tag{13}$$

where c is some constant. In the following we will omit the c-notation and will simply write, e.g., $\boldsymbol{n}$ instead of $\boldsymbol{n}_c$ or $\int_{\Omega_\varepsilon} \nabla_{\Gamma(t)} P \cdot \nabla_{\Gamma(t)} \varphi |\nabla\phi|$ instead of $\int_{\Omega_\varepsilon} \nabla_{\Gamma_c(t)} P \cdot \nabla_{\Gamma_c(t)} \varphi |\nabla\phi|$. Furthermore, for the sake of brevity and clarity, we will also assume that $\Omega_\varepsilon = \Omega$. While this assumption can be too restrictive for real 3D-applications, for our test purposes this assumption is justified. Interested readers are referred to works of Olshanskii et al. for the trace FEM [25] and/or for the space-time FEM [26, 24] which are high order accurate in space and time, stable, optimal with respect to d.o.f. and able to handle topological changes.

2.3. Numerical scheme for a surface-defined PDE

For the discretization in space we use time independent (conforming) bilinear finite elements with the corresponding space of test functions $Q_h = \text{span}\{\varphi_1, \ldots, \varphi_N\}$. For notational simplicity let us assume that the velocity field of the surface and the convection are autonomous, particularly $\boldsymbol{v} \neq \boldsymbol{v}(\rho)$ and $\boldsymbol{w} \neq \boldsymbol{w}(\rho)$. Then the weak formulation of (6) reads:

$$\begin{aligned} \int_\Omega \left(\partial_t^\bullet \rho + \rho \nabla_\Gamma \cdot \boldsymbol{v}\right) \varphi |\nabla\phi| \quad &= \quad \int_\Omega \Big(D \Delta_{\Gamma(t)} \rho - \nabla_{\Gamma(t)} \cdot (\boldsymbol{w}\rho) \Big) \varphi |\nabla\phi| \\ &+ \quad \int_\Omega g(\rho) \varphi |\nabla\phi|, \qquad \forall \varphi \in Q_h \,. \end{aligned} \tag{14}$$

After some derivations (see, e.g., [11] or [31] for details) we can rewrite (14) as follows

$$\begin{aligned} \frac{d}{dt} \int_\Omega \rho\varphi |\nabla\phi| \quad + \quad & \int_\Omega D \nabla_{\Gamma(t)} \rho \cdot \nabla_{\Gamma(t)} \varphi |\nabla\phi| - \int_\Omega \rho \boldsymbol{w} \cdot \nabla_{\Gamma(t)} \varphi |\nabla\phi| = \\ & \int_\Omega \rho \partial_t^\bullet \varphi |\nabla\phi| - \int_{\partial\Omega} \rho\varphi \boldsymbol{v} \cdot \boldsymbol{n}_{\partial\Omega} |\nabla\phi| + \int_\Omega g(\rho) \varphi |\nabla\phi| \,, \end{aligned}$$

where $\boldsymbol{n}_{\partial\Omega}$ is the outward normal vector to $\partial\Omega$. Since test functions are time independent, we obtain that

$$\partial_t^\bullet \varphi = \boldsymbol{v} \cdot \nabla\varphi$$

and therefore

$$\begin{aligned}\frac{d}{dt}\int_\Omega \rho\varphi|\nabla\phi| + \int_\Omega D\nabla_{\Gamma(t)}\rho\cdot\nabla_{\Gamma(t)}\varphi|\nabla\phi| \quad &- \quad \int_\Omega \rho\boldsymbol{w}\cdot\nabla_{\Gamma(t)}\varphi|\nabla\phi| = \\ \int_\Omega \rho\boldsymbol{v}\cdot\nabla\varphi|\nabla\phi| - \int_{\partial\Omega}\rho\varphi\boldsymbol{v}\cdot\boldsymbol{n}_{\partial\Omega}|\nabla\phi| \quad &+ \quad \int_\Omega g(\rho)\varphi|\nabla\phi|\,.\end{aligned}$$

In [31] the authors proposed and numerically studied the following implicit FCT-stabilized numerical scheme: given P^m, the FE coefficient vector of the solution's FE projection $\boldsymbol{P}^m = \sum_i P_i^m\varphi_i$, at the m-th time instance t^m and the time step $\Delta t = t^{m+1} - t^m$, we solve for P^{m+1} by the following equation

$$\begin{aligned}\frac{1}{\Delta t}\int_\Omega P^{m+1}\varphi|\nabla\phi^{m+1}| + \int_\Omega (D\nabla_{\Gamma^{m+1}}P^{m+1} \quad &- \quad \boldsymbol{w}^{m+1}P^{m+1})\cdot\nabla_{\Gamma^{m+1}}\varphi|\nabla\phi^{m+1}| \\ -\int_\Omega P^{m+1}\boldsymbol{v}^{m+1}\cdot\nabla\varphi|\nabla\phi^{m+1}| \quad &+ \quad \int_{\partial\Omega} P^{m+1}\varphi\boldsymbol{v}^{m+1}\cdot\boldsymbol{n}_{\partial\Omega}|\nabla\phi^{m+1}| \\ &= \quad \frac{1}{\Delta t}\int_\Omega P^m\varphi|\nabla\phi^m| \\ &+ \quad \int_\Omega g(\boldsymbol{P}^m)\varphi|\nabla\phi^m|\,, \qquad (15)\end{aligned}$$

for all $\varphi \in Q_h$. Using $S_h = Q_h$ as a space of ansatz-functions, the matrix formulation of equation (15) looks like follows:

$$\begin{aligned}\Big[\boldsymbol{M}\big(|\nabla\phi^{m+1}|\big) \quad &+ \quad \Delta t D\boldsymbol{L}\big(\Gamma^{m+1},|\nabla\phi^{m+1}|\big) - \Delta t\boldsymbol{K}\big(\Gamma^{m+1},\boldsymbol{w}^{m+1},|\nabla\phi^{m+1}|\big) \\ &- \quad \Delta t\boldsymbol{N}\big(\boldsymbol{v}^{m+1},|\nabla\phi^{m+1}|\big) + \Delta t\boldsymbol{R}\big(\boldsymbol{v}^{m+1},|\nabla\phi^{m+1}|\big)\Big]\,P^{m+1} \\ &= \boldsymbol{M}\big(|\nabla\phi^m|\big)P^m + \Delta t\boldsymbol{G}\big(\boldsymbol{P}^m,|\nabla\phi^m|\big)\,. \qquad (16)\end{aligned}$$

Here, $\boldsymbol{M}(\cdot)$ denotes the (consistent) mass matrix, $\boldsymbol{L}(\cdot)$ is the discrete Laplace-Beltrami operator, $\boldsymbol{K}(\cdot)$ is the discrete on-surface advection operator with the linearized velocity $\boldsymbol{w}^m$, $\boldsymbol{N}(\cdot)$ is the discrete operator due to the surface evolution

and $\boldsymbol{R}(\cdot)$ are discrete boundary integrals with the entries defined by the formulae

$$m_{ij}(\psi) = \int_\Omega \varphi_i\varphi_j\psi\,, \tag{17}$$

$$l_{ij}(\Gamma^{m+1},\psi) = \int_\Omega P_{\Gamma^{m+1}}\nabla\varphi_i\cdot\nabla\varphi_j\psi\,, \tag{18}$$

$$k_{ij}(\Gamma^{m+1},\boldsymbol{w}^{m+1},\boldsymbol{\psi}) = \int_\Omega \varphi_j\boldsymbol{w}^{m+1}\cdot P_{\Gamma^{m+1}}\nabla\varphi_i\psi\,, \tag{19}$$

$$G_i(\boldsymbol{P}^m,\psi) = \int_\Omega g(\boldsymbol{P}^m)\varphi_i\psi\,, \tag{20}$$

$$r_{ij}(\boldsymbol{v}^{m+1},\psi) = \int_{\partial\Omega} \varphi_j\varphi_i\boldsymbol{v}^{m+1}\cdot\boldsymbol{n}_{\partial\Omega}\psi\,, \tag{21}$$

$$n_{ij}(\boldsymbol{v}^{m+1},\psi) = \int_\Omega \varphi_j\boldsymbol{v}^{m+1}\cdot\nabla\varphi_i\psi\,. \tag{22}$$

2.4. Linearization of nonlinear reaction terms

As mentioned in the introductory section, pattern-forming mechanisms play a very important role in bio-medical applications. One of the driven factors of pattern occurrence is a Turing instability. In this paper we focus on systems of Turing-instability type. The reason is two-fold: on the one hand, there is a wide range of applications for such pattern-forming systems (see, e.g., protein-protein interaction on a cell membrane [29, 15]). On the other hand, these are convenient systems for us to verify the usability of our numerical scheme. In the following we consider the system of reaction-diffusion equations (4)–(5) with $\Gamma(t)$ being developed according to (3).

Turing systems are often characterized by intricately coupled nonlinear reaction terms. Hence their appropriate treatment in a numerical framework is an important task. In this paper we employ Taylor series expansion to handle the nonlinear reaction terms after splitting the time interval $T = [0, t_M]$ by discrete time instants $0 < t_1 < \ldots < t_M$ and denoting the time step size by $\Delta t = t_{m+1} - t_m$:

$$g_1(\rho_1^{m+1},\rho_2^{m+1}) \approx g_1(\rho_1^m,\rho_2^m) + \nabla g_1(\rho_1^m,\rho_2^m)\cdot\begin{pmatrix}\rho_1^{m+1}-\rho_1^m\\ \rho_2^{m+1}-\rho_2^m\end{pmatrix}, \tag{23}$$

$$g_2(\rho_1^{m+1},\rho_2^{m+1}) \approx g_2(\rho_1^m,\rho_2^m) + \nabla g_2(\rho_1^m,\rho_2^m)\cdot\begin{pmatrix}\rho_1^{m+1}-\rho_1^m\\ \rho_2^{m+1}-\rho_2^m\end{pmatrix}. \tag{24}$$

Herein the superscript m denotes the evaluation of the underlying function at the time instant $t = t_m$. We further assume that both $g_1(\cdot)$ and $g_2(\cdot)$ can be (naturally) prolongated from $\Gamma(t)$ to the outer region.

By employing the numerical scheme (16) together with formulas (23) and (24) we end up with a linear system of equations for the discrete solution $\boldsymbol{x}^{m+1} = (P_1^{m+1}, P_2^{m+1})^T$ where $P_{1,2}$ represent the FE coefficient vectors of $\rho_{1,2}$ as before:

$$A(\boldsymbol{x}_m)\boldsymbol{x}_{m+1} = b(\boldsymbol{x}_m)\,, \tag{25}$$

where the matrix $A(\cdot)$ on the left-hand-side and the vector $b(\cdot)$ on the right-hand-side are defined as

$$A(\boldsymbol{x}_m) = \begin{pmatrix} \boldsymbol{M} + \Delta t\Big(D_1^\rho \boldsymbol{L} - \boldsymbol{N} + \boldsymbol{R} - \boldsymbol{G}_1^{\rho_1}\Big) & -\Delta t \boldsymbol{G}_1^{\rho_2} \\ -\Delta t \boldsymbol{G}_2^{\rho_1} & \boldsymbol{M} + \Delta t\Big(D_2^\rho \boldsymbol{L} - \boldsymbol{N} + \boldsymbol{R} - \boldsymbol{G}_2^{\rho_2}\Big) \end{pmatrix}$$

and

$$b(\boldsymbol{x}_m) = \begin{pmatrix} \boldsymbol{M} P_1^m + \Delta t\Big(\boldsymbol{G}_1 - \boldsymbol{G}_1^{\rho_1} P_1^m - \boldsymbol{G}_1^{\rho_2} P_2^m\Big) \\ \boldsymbol{M} P_2^m + \Delta t\Big(\boldsymbol{G}_2 - \boldsymbol{G}_2^{\rho_1} P_1^m - \boldsymbol{G}_2^{\rho_2} P_2^m\Big) \end{pmatrix}.$$

Here, we use the notations (17)–(21) to define entries of matrices $\boldsymbol{M}$, $\boldsymbol{L}$, $\boldsymbol{N}$ and $\boldsymbol{R}$ and dropped their dependencies. Furthermore we define the discrete counterparts of the reaction terms as follows:

$$\begin{aligned}
\boldsymbol{G}_1 &= \boldsymbol{G}_1(\boldsymbol{P}_1^m, \boldsymbol{P}_2^m, |\nabla \phi^m|) \quad \text{with} \quad g_{1\,i}(\boldsymbol{P}_1^m, \boldsymbol{P}_2^m, \psi) = \int_\Omega g_1(\boldsymbol{P}_1^m, \boldsymbol{P}_2^m)\varphi_i \psi\,, \\
\boldsymbol{G}_2 &= \boldsymbol{G}_2(\boldsymbol{P}_1^m, \boldsymbol{P}_2^m, |\nabla \phi^m|) \quad \text{with} \quad g_{2\,i}(\boldsymbol{P}_1^m, \boldsymbol{P}_2^m, \psi) = \int_\Omega g_2(\boldsymbol{P}_1^m, \boldsymbol{P}_2^m)\varphi_i \psi\,, \\
\boldsymbol{G}_1^{\rho_1} &= \boldsymbol{G}_1^{\rho_1}(\boldsymbol{P}_1^m, \boldsymbol{P}_2^m, |\nabla \phi^m|) \quad \text{with} \quad g_{1_{ij}}^{\rho_1}(\boldsymbol{P}_1^m, \boldsymbol{P}_2^m, \psi) = \int_\Omega \partial_{\rho_1} g_1(\boldsymbol{P}_1^m, \boldsymbol{P}_2^m)\varphi_i \varphi_j \psi\,, \\
\boldsymbol{G}_1^{\rho_2} &= \boldsymbol{G}_1^{\rho_2}(\boldsymbol{P}_1^m, \boldsymbol{P}_2^m, |\nabla \phi^m|) \quad \text{with} \quad g_{1_{ij}}^{\rho_2}(\boldsymbol{P}_1^m, \boldsymbol{P}_2^m, \psi) = \int_\Omega \partial_{\rho_2} g_1(\boldsymbol{P}_1^m, \boldsymbol{P}_2^m)\varphi_i \varphi_j \psi\,, \\
\boldsymbol{G}_2^{\rho_1} &= \boldsymbol{G}_2^{\rho_1}(\boldsymbol{P}_1^m, \boldsymbol{P}_2^m, |\nabla \phi^m|) \quad \text{with} \quad g_{2_{ij}}^{\rho_1}(\boldsymbol{P}_1^m, \boldsymbol{P}_2^m, \psi) = \int_\Omega \partial_{\rho_1} g_2(\boldsymbol{P}_1^m, \boldsymbol{P}_2^m)\varphi_i \varphi_j \psi\,, \\
\boldsymbol{G}_2^{\rho_2} &= \boldsymbol{G}_2^{\rho_2}(\boldsymbol{P}_1^m, \boldsymbol{P}_2^m, |\nabla \phi^m|) \quad \text{with} \quad g_{2_{ij}}^{\rho_2}(\boldsymbol{P}_1^m, \boldsymbol{P}_2^m, \psi) = \int_\Omega \partial_{\rho_2} g_2(\boldsymbol{P}_1^m, \boldsymbol{P}_2^m)\varphi_i \varphi_j \psi\,.
\end{aligned}$$

The system (25) has to be solved in every time step.

Let us summarize the main algorithmic steps required to perform one iteration in time for finding the corresponding solutions at t_{m+1}:

1. Update the position of the surface $\Gamma(t_{m+1}) = \{\boldsymbol{x} : \phi(\boldsymbol{x}, t_{m+1}) = 0\}$ by solving the transport equation

$$\frac{\partial \phi}{\partial t} + \boldsymbol{v} \cdot \nabla \phi = 0$$

for the level set function $\phi(\boldsymbol{x}, t_{m+1})$. This is done by applying the finite element discretization in space and the implicit Euler discrization in time with optional flux corrected stabilization of the convective term $\boldsymbol{v} \cdot \nabla \phi$. The requirement of corresponding regularization/reinitialization techniques is out of the scope of this work. The analysis of a proper choice is highly demanding and problem dependent. For exemplary studies in this direction the interested reader is therefore kindly referred to corresponding literature, e.g., [36].

2. Calculate the gradient of the level set function $\nabla \phi^{m+1}$. Reassemble matrices, which depend on $|\nabla \phi^{m+1}|$ or $\boldsymbol{v}^{m+1}$. If necessary, perform linearization of the reactive terms.
3. Solve the system of linear equations (25) for the tuple $(\rho_1^{m+1}, \rho_2^{m+1})^T$.

3. Numerical results

Here we demonstrate the applicability of our coupled FE-LS scheme to selected examples. In the following section, Section 3.1, we validate the spatial convergence of our scheme by considering an example of a heat equation on a curve which is prescribed by the zero level set of the function $\phi(\boldsymbol{x}, t)$. In the next section, Section 3.2, we show the numerical solution of the Schnakenberg model on a nontrivial stationary surface in the three dimensional Euclidean space. Then, in Section 3.3 we demonstrate the coupling of the Koch-Meinhardt reaction-diffusion model of the Turing-instability type with the evolution of level sets, where the velocity is proportional to the numerical solution of the model.

3.1. Exemplary convergence study

In this section let us consider an exemplary study of the convergence of our FE-LS scheme. For validation purposes we solve the two dimensional heat

equation on a pulsating circle as already suggested by Dziuk and Elliott [11, Example 1]. The underlying domain Ω is an annular region with outer radius 1.5 and inner radius 0.5, e.g.,

$$\Omega \quad = \quad R_{0.5}^{1.5} = \left\{ \mathbf{x} = (x_1, x_2) \in \mathbb{R}^2 \,\middle|\, 0.5 < |\mathbf{x}| < 1.5 \right\} .$$

We prescribe an analytical reference solution

$$\rho^*(\mathbf{x}, t) \quad = \quad e^{-t/|\mathbf{x}|^2} \frac{x_1}{|\mathbf{x}|}$$

and solve the heat equation

$$\frac{\partial^* \rho(\mathbf{x}, t)}{\partial t} - \Delta_{\Gamma(t)} \rho(\mathbf{x}, t) \quad = \quad f \,,$$

where the right hand side f must be calculated accordingly. The pulsating circle is determined by the zero level sets of the following analytical reference function

$$\phi^*(\mathbf{x}, t) \quad = \quad |\mathbf{x}| - 1 + \sin(4t)(|\mathbf{x}| - 0.5)(1.5 - |\mathbf{x}|) \,.$$

This function is numerically approximated by solving the corresponding LS transport equation (3) starting with the initial solution $\phi(\mathbf{x}, 0) = \phi^*(\mathbf{x}, 0)$. Our FE discretization of (3) follows the regular Galerkin approach with first order implicit time integration (Implicit Euler). The transport velocity is determined to fit to the analytical reference solution, i.e., ϕ^* solves

$$\frac{\partial \phi^*}{\partial t} + \boldsymbol{v}^* \cdot \nabla \phi^* \quad = \quad 0 \,,$$

where $\boldsymbol{v}^* = (v_1^*, v_2^*)$ is given by

$$\begin{aligned} v_1^* \quad &= \quad -\frac{x_1}{|\mathbf{x}|} \frac{4\cos(4t)(|\mathbf{x}| - 0.5)(1.5 - |\mathbf{x}|)}{1 + 2\sin(4t)(1 - |\mathbf{x}|)} = -\frac{\phi_t^*}{\phi_{x_1}^*} x_1^2 / |\mathbf{x}|^2 \,, \\ v_2^* \quad &= \quad -\frac{x_2}{|\mathbf{x}|} \frac{4\cos(4t)(|\mathbf{x}| - 0.5)(1.5 - |\mathbf{x}|)}{1 + 2\sin(4t)(1 - |\mathbf{x}|)} = -\frac{\phi_t^*}{\phi_{x_2}^*} x_2^2 / |\mathbf{x}|^2 \,. \end{aligned}$$

For our simulations we use $\rho^*(\mathbf{x}, 0)$ as initial condition and monitor the numerical approximations to the analytical reference solution at a corresponding instance of time. The following numerical data is obtained after 100 time steps with a fixed time stepping of $\Delta t = 0.0001$. This choice accounts for the purpose

of documenting the numerical convergence in terms of the spatial discretization and neglecting errors in time. We monitor the numerical error to the reference solutions u^* and ϕ^*. In Figure 1 we track the L^2 and H^1 error of u in the annular region $R_{0.875}^{1.125}$ as we are mostly interested in the error close to our zero level set which is located at $|\mathbf{x}| \approx 0.99$. Figure 2 depicts the L^2_ϕ error of ρ, where

$$L^2_\phi(\Omega) \quad = \quad \left\{ v \,\middle|\, \langle v, v \rangle_\phi < \infty \right\}$$

with the following defintion of the inner product and induced norm (cf. [11])

$$\begin{aligned} \langle u, v \rangle_\phi &= \int_\Omega uv |\nabla \phi| \,, \\ ||u||_{L^2_\phi(\Omega)} &= \sqrt{\langle u, u \rangle_\phi} \,. \end{aligned}$$

Note that this norm is consistent with the definition of the mass matrix in (17). The choice of this norm is motivated by the anticipation that $|\nabla \phi|$ is large at the zero level set and nearly vanishes elsewhere. In this case L^2_ϕ is an approximation of $L^2(\Gamma)$. The next plots in Figure 3 document the L^2 and H^1 errors of the level set function ϕ in the restricted annular region $R_{0.875}^{1.125}$.

All figures validate the high order of spatial convergence, i.e., our scheme is of second order in L^2 and first order in H^1 for both solutions u and ϕ. This can be readily observed from the decline of the corresponding plots.

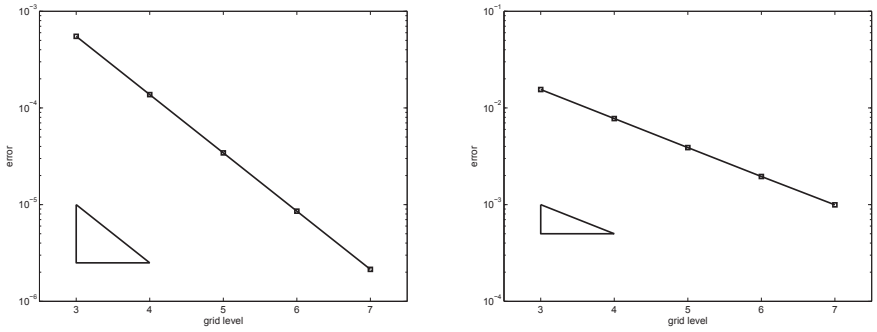

Figure 1: Reduction of the numerical L^2 (left) and H^1 (right) error of u in the annular strip $R_{0.875}^{1.125}$ for successive grid levels. The reference second and first order of convergence is visualized in terms of the bottom-left triangles, respectively.

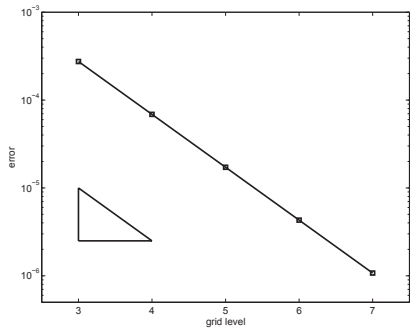

Figure 2: Reduction of the numerical L^2_ϕ error of u for successive grid levels. The reference second order of convergence is visualized in terms of the bottom-left triangle.

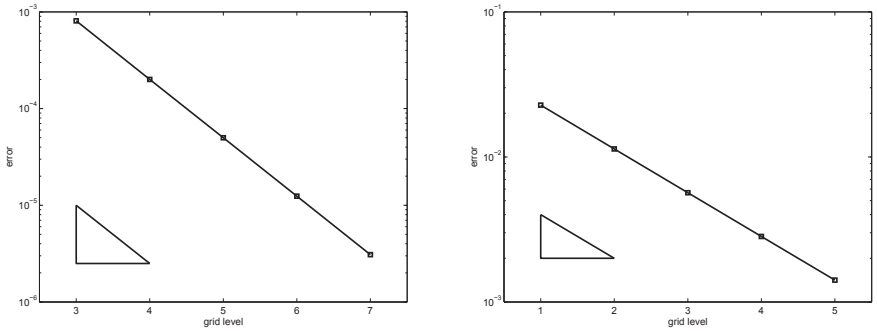

Figure 3: Reduction of the numerical L^2 (left) and H^1 (right) error of ϕ in the annular strip $R^{1.125}_{0.875}$ for successive grid levels. The reference second and first order of convergence is visualized in terms of the bottom-left triangles, respectively.

3.2. Schnakenberg model on a stationary surface

In this second example we consider the performance of our solver for models of the Turing-instability type of stationary surfaces. For this purpose we compute the numerical solution of the Schnakenberg model on a stationary surface Γ, which mathematically reads as follows

$$\frac{\partial \rho_1}{\partial t} = \Delta_\Gamma \rho_1 + \gamma(a - \rho_1 + \rho_1^2 \rho_2)\,, \tag{26}$$

$$\frac{\partial \rho_2}{\partial t} = D\Delta_\Gamma \rho_2 + \gamma(b - \rho_1^2 \rho_2)\,. \tag{27}$$

For the underlying domain Ω we choose the cube $\Omega = (-2.5, 2.5)^3$. The zero level set of the function $\phi(\cdot)$ implicitly prescribes the stationary surface Γ of an animal-like geometry. The presented numerical results are courtesy of Marcel Penstorf [28].

For certain parameter settings it is known that the solution $(\rho_1, \rho_2)^T$ of the system (26)–(27) reveals instabilities due to Turing-type effects. The objective of our following numerical assay is to verify that our FE-LS scheme can capture these instabilities.

Our configuration reads as follows: We take

$$a = 1.0, \quad b = 1.0,$$

and set the initial condition as a randomly small perturbation from the steady state point $(2, 0.25)^T$. We start from the time point $t = 0$ and proceed in time with the time step $\Delta t = 0.005$ until $t = 1.0$, i.e., performing 200 iteration steps. For the parameter setting $\gamma = 25$, $D = 5$ we observe that the numerical solution retains the steady state (results omitted). However for $\gamma = 25$ and $D = 10$ the solution promotes patterns, see Figures 4(c) and 4(d).

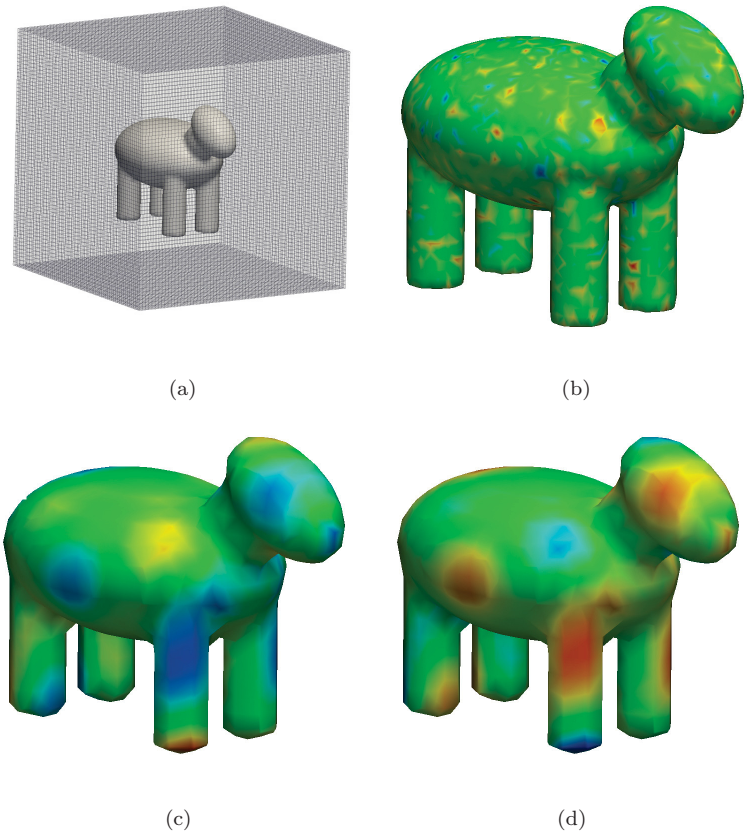

Figure 4: (a) Mesh with an embedded zero-level set prescription of Γ; (b) Initial condition for ρ_1; (c) values of ρ_1 and (d) values of ρ_2 at $t = 1.0$ for the parameter-setting $\gamma = 25.0$, $D = 10.0$.

3.3. Brusselator model on an evolving surface

We consider the following reaction-diffusion model which is referred to as the linearized Brusselator [6]:

$$\frac{\partial \rho_1}{\partial t} = \alpha_1 \rho_1 \left(1 - r_1 {\rho_2}^2\right) - \rho_2 \left(1 - r_2 \rho_1\right) + D^{\rho_1} \Delta_{\Gamma(t)} \rho_1 \,, \tag{28}$$

$$\frac{\partial \rho_2}{\partial t} = \beta_1 \rho_2 \left(1 + \frac{\alpha_1 r_1}{\beta_1} \rho_1 \rho_2\right) + \rho_1 \left(\gamma_1 - r_2 \rho_2\right) + D^{\rho_2} \Delta_{\Gamma(t)} \rho_2 \,, \tag{29}$$

where the surface $\Gamma(t)$ is the unit circle situated at the origin of the coordinate system. The surface evolves in time with the velocity field $\boldsymbol{v}$. Again, it is known

that under certain conditions on the parameters this reaction-diffusion model exhibits a Turing instability.

This example shall prove that our FE-LS scheme allows for studying complex pattern formations on a surface those deformation is modulated by the solution of a PDE system. Therefore we choose the velocity $\boldsymbol{v}$ of $\Gamma(t)$ to be proportional to ρ_1, i.e., we set

$$\boldsymbol{v} \quad = \quad 0.01\,\rho_1\,\boldsymbol{n} \tag{30}$$

with $\boldsymbol{n} = \nabla\phi(\boldsymbol{x},t)/|\nabla\phi(\boldsymbol{x},t)|$ denoting the outward normal to a certain level set. While solving the transport equation for the level set function ϕ, we assume that its zero level set is located at a significant distance away from $\partial\Omega$ and therefore the boundary $\partial\Omega$ does not influence a position of $\Gamma(t_{m+1}) = \{\boldsymbol{x} \,:\, \phi(t_{m+1},\boldsymbol{x}) = 0\}$ during the time point t_{m+1} (i.e., no prescription of ϕ on $\partial\Omega$ is required). We choose the annular region $R_{0.5}^{1.5}$ as underlying domain as its inner and outer boundaries are aligned with some initial level set $\Gamma_r(t=0) = \{\boldsymbol{x}\,|\,\phi(\boldsymbol{x},t=0) = r\}$.

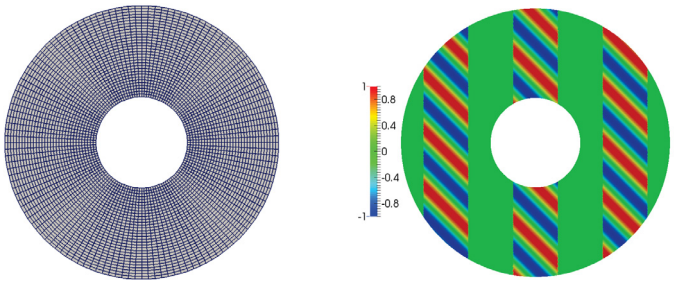

(a) mesh (b) $\rho_1(\boldsymbol{x},t=0)$

Figure 5: (a) Mesh of a four-fold refinement, (b) initial condition for ρ_1.

The parameter setting in (28)–(29) is taken to be as follows

$$D^{\rho_1} = 0.88\,\delta\,, \qquad D^{\rho_2} = 5.16\,\delta\,,$$

$$\delta = 0.0045\,, \qquad \gamma_1 = -0.899\,,$$

$$\alpha_1 = 0.899\,, \qquad \beta_1 = -0.91\,.$$

The time-step is taken to be $\Delta t = 0.001$. For the spatial discretization we use an 'almost' uniform mesh of 262 144 quadrilaterals which corresponds to a seven-fold mesh refinement. This level of refinement results in an overall of 263 168 degrees of freedom. Exemplarily, in Figure 5(a) we depict the level 4 mesh resulting from a four-fold mesh refinement. As a particular example of emergence of complicated patterns we choose the following sinusoidal initial conditions for ρ_1 and ρ_2, see Figure 5(b),

$$\rho_1(\boldsymbol{x})\,|_{t=0} = \begin{cases} \sin\Big(10(x_1+x_2)\Big), & \text{if } x_1 \in [-1.25,-0.75]\cup[-0.25,0.25]\cup[0.75,1.25] \\ 0, & \text{else}\,, \end{cases}$$

$$\rho_2(\boldsymbol{x})\,|_{t=0} = \begin{cases} \cos\Big(10(x_1+x_2)\Big), & \text{if } x_1 \in [-1.25,-0.75]\cup[-0.25,0.25]\cup[0.75,1.25] \\ 0, & \text{else}\,. \end{cases}$$

Concerning the evolution of the level set function $\phi(\cdot)$, we solve the LS transport equation (3) with the velocity as defined above in equation (30). Initially we prescribe the solution $\phi(\boldsymbol{x}, 0)$ to satisfy

$$\phi(\boldsymbol{x}, 0) = |\boldsymbol{x}| - 1.0\,. \tag{31}$$

The coupling of (28)–(29) with the transport equation (3) through (30) leads to the deformation of the level sets Γ_r which in turn influences the system (28)–(29). Figure 6 depicts the dynamics of the numerical solution for ρ_1 and ϕ in a Γ-band of width 0.15. As time evolves we recognize a strong deformation of the level sets in the vicinity of large values of the solution ρ_1 as expected by the choice of the LS velocity (30).

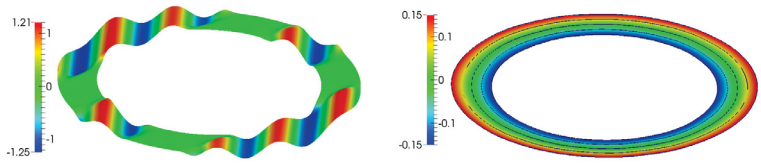

(a) ρ_1 at $t = 0.2$ (b) level set ϕ at $t = 0.2$

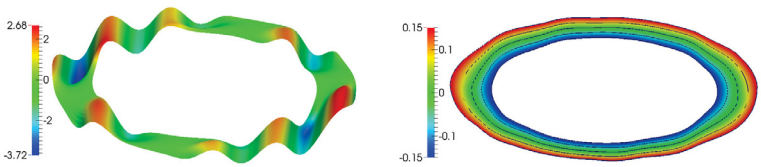

(c) ρ_1 at $t = 1.0$ (d) level set ϕ at $t = 1.0$

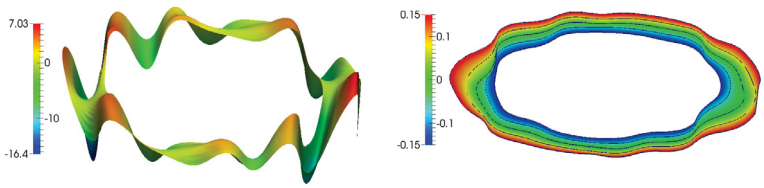

(e) ρ_1 at $t = 2.0$ (f) level set ϕ at $t = 2.0$

Figure 6: Numerical solutions for ρ_1 and ϕ in the ε-band Ω_ε of the width $\varepsilon = 0.15$ at distinct time points.

4. Conclusion

In this article we presented a numerical framework for systems of the reaction-diffusion equations on evolving-in-time surfaces. The proposed framework com-

bines the level set methodology for the implicit description of the time dependent surface $\Gamma = \Gamma(t)$, the Eulerian finite element formulation for the numerical treatment of partial differential equations and, if required, the flux-corrected transport scheme for the numerical stabilization of arising advective, resp., convective terms.

Our numerical results support the reliability of the proposed computational framework in terms of numerical convergence and capturing of typical/expected solution profiles. We have thus developed an approach that can readily be employed for biological applications that involve PDEs on evolving surfaces.

As we suggested in Section 3.2, our framework is also applicable to three dimensional models which is mandatory when considering real-life applications. Since the computational and analytical complexity significantly increases in three dimensional cases, detailed numerical investigations are subject of forthcoming work.

Acknowledgments

Ramzan Ali is supported by a DAAD/UCA PhD scholarship program with grant number $A/12/93809$.

References

[1] M. Aida, T. Tsujikawa, M. Efendiev, A. Yagi, M. Mimura, Lower estimate of the attractor dimension for a chemotaxis growth system, J. London Math. Soc. 740 (2006) 453–474.

[2] D. Ambrosi, F. Bussolino, L. Preziosi, A review of vasculogenesis models., Comput. Math. Meth. Medicine: An Interdisciplinary Journal of Mathematical, Theo. Clin. Asp Med. 6 (2005) 1–19.

[3] A.R.A. Anderson, M.A.J. Chaplain, Continuous and discrete mathematical models of tumor-induced angiogenesis, Bull. Math. Bio. 60 (1998) 857–899.

[4] A.R.A. Anderson, M.A.J. Chaplain, E.L. Newman, R.J.C. Steele, A.M. Thompson, Mathematical modelling of tumour invasion and metastasis, Annals Phys. 2 (1999) 129–154.

[5] R. Barreira, C.M. Elliott, A. Madzvamuse, The surface finite element method for pattern formation on evolving biological surfaces, J. Math. Bio. 63 (2011) 1095–1119. Cited By (since 1996)11.

[6] M. Bergdorf, I.F. Sbalzarini, P. Koumoutsakos, A lagrangian particle method for reaction-diffusion systems on deforming surfaces, J. Math. Bio. 61 (2010) 649–663. Cited By (since 1996)12.

[7] M.A. Chaplain, A.M. Stuart, A model mechanism for the chemotactic response of endothelial cells to tumour angiogenesis factor., IMA J. Math. App. Med. Bio. 10 (1993) 149–168.

[8] M.A.J. Chaplain, Mathematical modelling of angiogenesis, J. Neuro-Oncology 50 (2000) 37–51.

[9] M.A.J. Chaplain, S.R. McDougall, A.R.A. Anderson, Mathematical modeling of tumor-induced angiogenesis, Ann. Rev. Bio. Engg 8 (2006) 233–257.

[10] J. Condeelis, R.H. Singer, J.E. Segall, The great escape: When cancer cells hijack the genes for chemotaxis and motility, Ann. Rev. Cell Dev. Bio. 21 (2005) 695–718. Cited By (since 1996)170.

[11] G. Dziuk, C.M. Elliott, An eulerian approach to transport and diffusion on evolving implicit surfaces, Comput. Vis. Sci. 13 (2010) 17–28.

[12] C.M. Elliott, B. Stinner, C. Venkataraman, Modelling cell motility and chemotaxis with evolving surface finite elements, J. Roy. Soc. Interf. 9 (2012) 3027–3044.

[13] S.F. Frisken, R.N. Perry, A. Rockwood, T. Jones, Adaptively sampled fields: A general representation of shape for computer graphics, 2006.

[14] A. Gamba, D. Ambrosi, A. Coniglio, A.D. Candia, S.D. Talia, E. Giraudo, G. Serini, L. Preziosi, F. Bussolino, Percolation, morphogenesis, and burgers dynamics in blood vessels formation, Phys. Rev. Lett. 90 (2003) 118101/1–118101/4.

[15] A. Goryachev, A. Pokhilko, Dynamics of cdc42 network embodies a turing-type mechanism of yeast cell polarity, FEBS Letters 582 (2008) 1437–1443.

[16] G. Hetzer, A. Madzvamuse, W. Shen, Characterization of turing diffusion-driven instability on evolving domains, Disc. Cont. Dyn. Sys- A 32 (2012) 3975–4000.

[17] E.F. Keller, L.A. Segel, Initiation of slime mold aggregation viewed as an instability, J. Theo. Bio. 26 (1970) 399–415.

[18] E.F. Keller, L.A. Segel, Model for chemotaxis, J. Theo. Bio. 30 (1971) 225–234.

[19] C. Landsberg, F. Stenger, A. Deutsch, M. Gelinsky, A. Rsen-Wolff, A. Voigt, Chemotaxis of mesenchymal stem cells within 3d biomimetic scaffolds-a modeling approach, J. Bio. 44 (2011) 359–364.

[20] M. Mimura, T. Tsujikawa, Aggregating pattern dynamics in a chemotaxis model including growth, Physica A: Stat. Mech. App. 230 (1996) 499–543.

[21] J. Murray, Mathematical biology i: An introduction, Springer Verlag, Third Edition (2002).

[22] J.D. Murray, Discussion: Turing's theory of morphogenesis - its influence on modelling biological pattern and form, Bull. Math. Bio. 52 (1990) 119–152.

[23] J.D. Murray, Mathematical biology ii: Spatial models and biomedical applications, Springer Verlag (2003).

[24] M. Olshanskii, A. Reusken, Error analysis of a space-time finite element method for solving pdes on evolving surfaces, SIAM J. Numm. Anal. 52 (2014) 2092–2120.

[25] M. Olshanskii, A. Reusken, J. Grande, A finite element method for elliptic equations on surfaces, SIAM J. Numm. Anal. 47 (2009) 3339–3358.

[26] M. Olshanskii, A. Reusken, X. Xu, An eulerian space-time finite element method for diffusion problems on evolving surfaces, SIAM J. Numm. Anal. 52 (2014) 1354–1377.

[27] H. Park, J. Wu, Y. Rao, Molecular control of neuronalmigration, Bioessays 24 (2002) 821827.

[28] M. Penstorf, Die level-set-methode fuer reaktions-diffusions-gleichungen auf statischen oberflaechen, 2014.

[29] A. Raetz, M. Roeger, Turing instabilities in a mathematical model for signaling networks, J. Math. Bio. 65 (2012) 1215–1244.

[30] G. Serini, D. Ambrosi, E. Giraudo, A. Gamba, L. Preziosi, F. Bussolino, Modeling the early stages of vascular network assembly, EMBO J. 22 (2003) 1771–1779.

[31] A. Sokolov, R. Ali, S. Turek, An afc-stabilized implicit finite element method for partial differential equations on evolving-in-time surfaces, J. Comput. App. Math. (2015) 105–115.

[32] H.A. Stone, A simple derivation of the timedependent convective diffusion equation for surfactant transport along a deforming interface, Phys.Fluids A2 111 (1990) 335–362.

[33] R. Strehl, A. Sokolov, D. Kuzmin, D. Horstmann, S. Turek, A positivity-preserving finite element method for chemotaxis problems in 3d, J. Comput. Appl. Math. 239 (2013) 290–303.

[34] R. Strehl, A. Sokolov, D. Kuzmin, S. Turek, A flux-corrected finite element method for chemotaxis problems, Comput. meth. appl. math. 10 (2010) 219–232.

[35] L. Tian, C.B. Macdonald, S.J. Ruuth, Segmentation on surfaces with the closest point method, 2009.

[36] S. Turek, O. Mierka, S. Hysing, D. Kuzmin, Numerical study of a high order 3D FEM–level set approach for immiscible flow simulation, Comput. Meth. App. Sci. 27 (2013) 65–70.

[37] A. Turing, The chemical basis of morphogenesis, Phil Trans B 337 (1952) 37–72.

[38] R. Tyson, S.R. Lubkin, J.D. Murray, A minimal mechanism for bacterial pattern formation, Proceedings of the Royal Society B: Biological Sciences 266 (1999) 299–304.

[39] R. Tyson, S.R. Lubkin, J.D. Murray, Model and analysis of chemotactic bacterial patterns in a liquid medium, J. Math. Bio. 38 (1999) 359–375.

[40] R. Tyson, L. Stern, R. LeVeque, Fractional step methods applied to a chemotaxis model, J. Math. Bio. 41 (2000) 455–475.

[41] V. Vanag, I. Epstein, Pattern formation mechanisms in reaction-diffusion systems, Int. J. Dev. Bio. 53 (2009) 673–681.

[42] D. Wu, Signaling mechanisms for regulation of chemotaxis, Cell Res. 15 (2005) 52–56.

[43] G. Yngve, G. Turk, Creating smooth implicit surfaces from polygonal meshes, 2006.